

High-pressure structural, elastic, and electronic properties of the scintillator host material KMgF_3

G. Vaitheeswaran,^{1,*} V. Kanchana,¹ Ravhi S. Kumar,² A. L. Cornelius,² M. F. Nicol,² A. Svane,³
A. Delin,¹ and B. Johansson^{1,4}

¹*Applied Materials Physics, Department of Materials Science and Engineering, Royal Institute of Technology, Brinellvägen 23, 100 44 Stockholm, Sweden*

²*High Pressure Science and Engineering Center and Department of Physics, University of Nevada, Las Vegas, Nevada 89154, USA*

³*Department of Physics and Astronomy, University of Aarhus, DK-8000 Aarhus C, Denmark*

⁴*Condensed Matter Theory Group, Department of Physics, Uppsala University, Box 530, SE-751 21 Uppsala, Sweden*

(Received 21 March 2007; published 13 July 2007)

The high-pressure structural behavior of the fluoroperovskite KMgF_3 is investigated by theory and experiment. Density functional calculations were performed within the local density approximation and the generalized gradient approximation for exchange and correlation effects, as implemented within the full-potential linear muffin-tin orbital method. *In situ* high-pressure powder x-ray diffraction experiments were performed up to a maximum pressure of 40 GPa using synchrotron radiation. We find that the cubic $Pm\bar{3}m$ crystal symmetry persists throughout the pressure range studied. The calculated ground state properties—the equilibrium lattice constant, bulk modulus, and elastic constants—are in good agreement with experimental results. By analyzing the ratio between the bulk and shear moduli, we conclude that KMgF_3 is brittle in nature. Under ambient conditions, KMgF_3 is found to be an indirect gap insulator, with the gap increasing under pressure.

DOI: [10.1103/PhysRevB.76.014107](https://doi.org/10.1103/PhysRevB.76.014107)

PACS number(s): 71.15.Nc, 62.50.+p, 62.20.Dc, 61.10.Nz

I. INTRODUCTION

KMgF_3 is a technologically important fluoroperovskite. For example, it is used as a vacuum-ultraviolet-transparent material for lenses in optical lithography steppers¹ and in electro-optical applications.^{2,3} When doped with lanthanide ions, it is a very promising material for scintillators⁴ and radiation dosimeters.^{5,6} In addition, the physical properties of KMgF_3 may have implications for understanding the Earth's lower mantle.^{7,8}

KMgF_3 was first synthesized by van Arkel⁹ and has a simple cubic perovskite structure at room temperature.¹⁰ KMgF_3 demonstrates great stability under high compression and has not been found to undergo any phase transition at any temperature or pressure, suggesting it may be used as an internal x-ray calibrant.¹¹

Several experimental studies of the ground state properties of KMgF_3 have been performed. The elastic constants at ambient pressure have been measured by Rosenberg and Wigmore¹² and by Reshchikova,¹³ while Jones investigated their pressure and temperature dependences.¹⁴

From the theoretical side, electronic structure calculations for KMgF_3 have been carried out by means of linear combination of atomic orbitals,¹⁵ including the effects of doping with transition metal impurities in KMgF_3 .¹⁶ The electronic structures of divalent $3d$ transition metal impurities doped in KMgF_3 have been investigated by the pseudopotential method,¹⁷ and the properties of vacancies were studied by Hartree-Fock cluster calculations.¹⁸ The structural, electronic, and optical properties of KMgF_3 were recently investigated by the full-potential linear augmented plane wave (FP-LAPW) method.¹⁹

The present work is a combined theoretical and experimental study of the ground state and high-pressure properties of KMgF_3 . We present the equation of state resulting from high-pressure diamond-anvil cell experiments on KMgF_3 up

to 40 GPa. We also present the equation of state, the elastic constants, and the electronic structure from theoretical calculations using two different approximations for the exchange-correlation functional.

The remainder of the paper is organized as follows. Details of the computational method as well as details of the experimental setup are outlined in Sec. II. The measured and calculated equations of state are presented in Sec. III together with calculated ground state properties and elastic properties. The electronic structure and the pressure variation of the band gap are discussed in Sec. IV. Finally, conclusions are given in Sec. V.

II. COMPUTATIONAL AND EXPERIMENTAL DETAILS

A. Electronic structure method

The all-electron full-potential linear muffin-tin orbital (FP-LMTO) method²⁰ is used to calculate the total energies and basic ground state properties of KMgF_3 presented here. In this method, the crystal volume is split into two regions: nonoverlapping muffin-tin spheres surrounding each atom, and the interstitial region between the spheres. We used a double κ *spdf* LMTO basis (each radial function within the spheres is matched to a Hankel function in the interstitial region) to describe the valence bands. In the calculations, we included the $3s$, $3p$, $4s$, $4p$, and $3d$ bases for potassium, the $3s$, $2p$, $3p$, and $3d$ bases for magnesium, and the $2s$ and $2p$ bases for fluorine. The exchange-correlation potential was calculated within the local density approximation²¹ (LDA) as well as the generalized gradient approximation (GGA) scheme.²² The charge density and potential inside the muffin-tin spheres were expanded in terms of spherical harmonics up to $l_{max}=6$, while in the interstitial region, they were expanded in plane waves, with 14 146 waves (energy up to 156.30 Ry) included in the calculation. Total energies

were calculated as a function of volume for a $(16 \times 16 \times 16)$ k mesh containing 165 k points in the irreducible wedge of the Brillouin zone and were fitted to the Birch equation of state²³ to obtain the ground state properties.

The elastic constants were obtained from the variation of the total energy under volume conserving strains, as outlined in Refs. 24 and 25.

B. Experimental details

The high-pressure x-ray diffraction measurements used a sample of polycrystalline KMgF_3 prepared by the solid state reaction method from high purity constituent materials as described elsewhere in several reports.^{26–28} Diffraction patterns collected at ambient temperature and pressure showed a cubic ($Pm\bar{3}m$) symmetry with a cell parameter $a = 4.0060(2)$ Å for KMgF_3 which closely agrees with earlier reports.^{30,36} High pressures were generated by a Merrill-Bassett type diamond-anvil cell. A $185 \mu\text{m}$ sample chamber was formed in a rhenium metal gasket with a preindention of $60 \mu\text{m}$ thickness. The powder sample was loaded in the gasket with a few ruby grains and silicone fluid as pressure transmitting medium.³¹ Diffraction experiments were performed at the 16ID-B undulator beamline of the High Pressure Collaborative Access Team (HPCAT) of the Advanced Photon Source. A monochromatic x-ray beam with a wavelength of 0.4218 Å was focused down to a size of $30 \times 30 \mu\text{m}$. Diffraction images were collected with an image plate detector for an exposure time of 10 s. The distance between the sample and the detector and the inclination angle of the image plate were calibrated using a CeO_2 standard.

The two dimensional images were subsequently integrated to one dimensional diffraction patterns using the FIT2D software.³² The cell parameters were obtained by analyzing the diffraction patterns with the JADE software package, and the P - V data obtained were fitted with a second-order Birch-Murnaghan²³ equation of state. The standard ruby fluorescence technique and the newly proposed ruby pressure scale of Holzapfel³³ were used to obtain the pressures in the sample chamber.

III. GROUND STATE AND ELASTIC PROPERTIES

Powder x-ray diffraction patterns collected at several pressures are shown in Fig. 1. On compression, the diffraction patterns remain unchanged up to 40 GPa, except for the shifts of diffraction lines caused by the decreasing lattice constant. This implies that no structural transformations occur up to 40 GPa in KMgF_3 . Figure 2 shows the measured equation of state of KMgF_3 and compares it with theoretical curves calculated within the LDA and GGA. A better theoretical description is obtained with the LDA, which is somewhat surprising, since usually the GGA provides an improvement over LDA. At low pressures, the LDA volume is slightly smaller than the experimental one, while the situation reverses at high pressures, i.e., altogether the LDA predicts KMgF_3 to be stiffer than experimental observations. GGA, on the other hand, greatly overestimates the equilib-

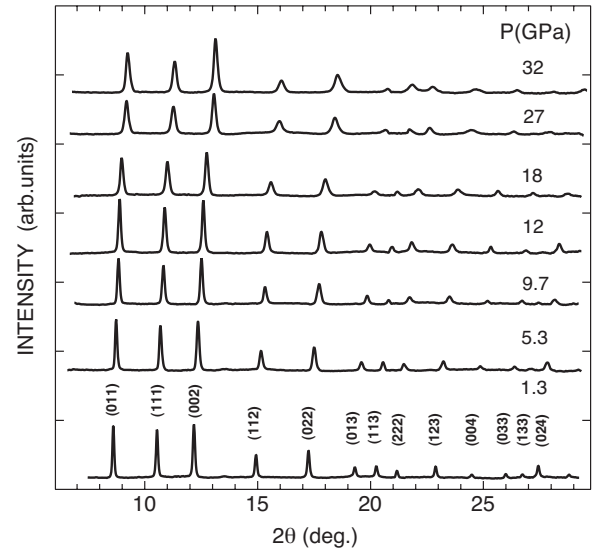


FIG. 1. Powder x-ray diffraction patterns recorded at various pressures up to 32 GPa. The indexing in terms of the simple cubic structure is given.

rium volume at ambient pressure, which is the main reason for the poor agreement with experiment. If the GGA curve is scaled throughout the pressure range with the error in equilibrium volume at $P=0$, nearly perfect agreement is found with experiment (not shown).

The lattice constant and bulk modulus measured in the present work as well as values calculated within the LDA and GGA approximations are given in Table I. Results from earlier experimental and theoretical works are quoted for comparison. The bulk modulus obtained in our experiments $B_0 = 71.2(2)$ GPa with $B'_0 = 4.7(3)$ compares well with other experimental results listed in Table I and also with NaMgF_3

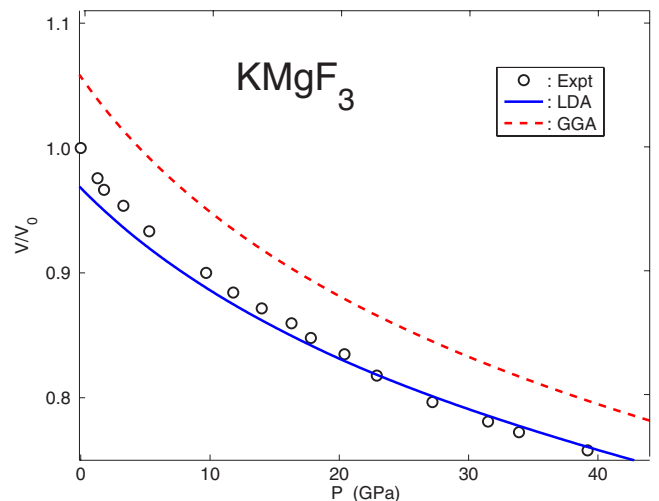


FIG. 2. (Color online) Equation of state of KMgF_3 in the pressure range from 0 to 40 GPa. The experimental data points are marked by circles, while theoretical results obtained with LDA and GGA are shown as full (blue) and dashed (red) curves. Volumes are given relative to the experimental equilibrium volume $V_0 = 64.288$ Å³.

TABLE I. Calculated lattice constants (in Å) and bulk modulus B_0 (in GPa) and its pressure derivative B'_0 of KMgF_3 at the theoretical equilibrium volume compared with the experiment and other theoretical calculations. The bulk moduli have been calculated both at the experimental and theoretical volumes [$B_0(V_0^{\text{exp}})$ and $B_0(V_0^{\text{th}})$, respectively].

	Lattice constant	$B_0(V_0^{\text{th}})$	$B_0(V_0^{\text{exp}})$	B'_0
GGA ^a	4.0809	72.01	97.85	4.65
LDA ^a	3.9630	91.47	83.23	4.79
LDA, LAPW ^b	3.91	90.97		4.64
Experiment	4.0060(2), ^a 3.973, ^c 3.978±0.05, ^d 3.9897, ^e 3.993, ^f 3.9839 ^g		71.2(2), ^a 70.4, ^h 75.1, ⁱ 75.6 ^j	4.7(3) ^a

^aPresent work.

^bReference 19.

^cReference 10.

^dReference 34.

^eReference 36.

^fReference 35.

^gReference 29.

^hReference 12.

ⁱReference 13.

^jReference 14.

reported recently by Liu *et al.*³⁷ [$B=76.0(1.1)$ GPa]. The lattice constant obtained within the LDA is 1.1% lower than the experimental value, while the corresponding bulk modulus is 22% higher than the experimental value, which is the usual kind of accuracy of LDA. However, the calculated LDA lattice constant from the present work agrees quite well with the experimental work when compared to the earlier FP-LAPW(LDA) calculations, in which the reported lattice constant is 2.4% lower than the experimental value.¹⁹ The LDA bulk modulus obtained from the present calculation agrees well with the value obtained by the FP-LAPW(LDA) method. When comparing the results obtained within GGA, the lattice constant is 1.9% higher than the experimental value, whereas our results for the bulk modulus are within the spread of the experimental data. This truly excellent agreement regarding the bulk modulus is, however, a bit fortuitous. Since the calculated equilibrium volume is overestimated with GGA (and underestimated with LDA), an error—solely depending on the error in volume—is introduced in the calculated bulk modulus. Therefore, we recalculated the bulk modulus also at the experimental volume in a manner similar to our earlier work³⁸ (see Table I). We find that this diminishes the discrepancies between the LDA and GGA results, as expected. In addition, the LDA bulk modulus now becomes *smaller* than the GGA one for KMgF_3 , and both functionals are seen to actually overestimate the bulk modulus, by approximately 14% (LDA) and 34% (GGA).

The present experiments on KMgF_3 relate to recent experiments performed for NaMgF_3 and alloys of NaMgF_3 and KMgF_3 . The crystal chemistry of $\text{Na}_{1-x}\text{K}_x\text{MgF}_3$ and NaMgF_3 was studied in detail at ambient and at high pressures by Zhao *et al.*^{27,39} NaMgF_3 undergoes a reversible phase transition from orthorhombic ($Pbnm$) to tetragonal ($P4/mbm$) and then to cubic structure ($Pm\bar{3}m$) upon compression. These phase transitions require either compositional changes, by increasing the K concentration to 40%, or

changing temperature or pressure. The structural changes in these perovskites are due to octahedral tiltings and shortening of Mg-F bonds compared to the cubic phase. A direct transformation from orthorhombic to cubic structure in NaMgF_3 , however, requires a very high temperature (1038 K). Moreover, the transition temperature is reported to increase with pressure. The temperature dependence of the crystal structure of KMgF_3 was recently investigated by neutron powder diffraction by Wood *et al.*¹¹ from 4.2 to 1223 K, and the cubic symmetry was found to be stable throughout this temperature range. The thermal expansion as well as the atomic displacement parameters obtained in their experiments show that the F ions behave less anisotropically than in NaMgF_3 at such high temperatures. On comparing these results with the present high-pressure diffraction experiments on KMgF_3 , one may speculate that application of pressure alone would not be sufficient to induce structural changes in KMgF_3 as the cubic phase is very stable. Such a phase transformation, if any, would require either application of very high temperature or a composition change in the system to achieve changes in the order parameters. Asbrink *et al.*⁴⁰ have studied single crystals of the transition metal bearing perovskite KMnF_3 , which is isostructural to KMgF_3 , under high pressure and observed a cubic-to-tetragonal phase transition at a critical pressure of 3.1 GPa. On combining these results, phase transitions from the cubic symmetry may be expected with a combination of composition change, temperature, and pressure in KMgF_3 . A systematic study on the octahedral tilting and order parameters with other dopant compositions and the effect of external thermodynamical variables are further required to understand the phase stability of KMgF_3 .

The elastic constants of KMgF_3 calculated within LDA and GGA are listed in Table II where they are also compared to experimental results as well as earlier calculations. The LDA overestimates all of the C_{11} , C_{12} , and C_{44} elastic constants by between 10% and 22% compared to

TABLE II. Calculated elastic constants, shear modulus (G), and Young's modulus (E) all expressed in GPa, and Poisson's ratio ν of KMgF_3 at the theoretical equilibrium volume.

	C_{11}	C_{12}	C_{44}	G	E	ν	Reference
GGA	137.0	39.5	54.6	52.3	126.3	0.208	Present work
LDA	177.0	48.7	58.7	60.9	149.5	0.228	Present work
LDA	119.26	38.26	63.23				19
Experiment	132 ± 1.5	39.6 ± 1.5	48.5 ± 0.6				12
	138 ± 0.2	43.6 ± 0.2	49.83 ± 0.08				13
	138.5 ± 0.5	44.1 ± 0.5	50.01 ± 0.1				14

experiment.¹²⁻¹⁴ The elastic constants obtained within GGA are much closer to the experimental values than are the LDA results. For instance, both C_{11} and C_{12} are within the experimental spread. Of course, the elastic constants also depend sensitively on the volume, and, therefore, the same argument as for the bulk modulus can be applied here. We have, however, refrained from recalculating all the elastic constants with the volume correction, but wish to mention that the excellent agreement between experiment and the GGA elastic constants should be interpreted with care. Another point of caution is the fact that the calculated values pertain to 0 K, while experiments are performed at room temperature. Finite temperature generally tends to reduce the elastic constants because of thermal expansion. Using the calculated elastic constants, we calculated the anisotropy factor $A = 2C_{44}/(C_{11} - C_{12})$. We find an $A = 0.91$ for LDA and $A = 1.12$ for GGA. The experimental result is 1.05, measured at room temperature,¹²⁻¹⁴ which is closer to but lower than the GGA value. However, the anisotropy factor is found to decrease as the temperature is lowered.¹³

A simple relationship, which empirically links the plastic properties of materials with their elastic moduli, was proposed by Pugh.⁴¹ The shear modulus G represents the resistance to plastic deformation, while the bulk modulus B represents the resistance to fracture. A high B/G ratio is associated with ductility, whereas a low value corresponds to brittle nature. The critical value which separates ductile and brittle materials is around 1.75; i.e., if $B/G > 1.75$, the material behaves in a ductile manner; otherwise, the material behaves in a brittle manner. Frantsevich *et al.*,⁴² in a similar

fashion, have suggested $B/G \sim 2.67$ as the critical value separating brittle and ductile behaviors. In the case of KMgF_3 , the calculated value of B/G is 1.5 within LDA and 1.4 within GGA, hence classifying this material as brittle.

Pettifor⁴³ suggested that the angular character of atomic bonding in metals and compounds, which also relates to the ductility, could be described by the Cauchy pressure $C_{12} - C_{44}$. For metallic bonding, the Cauchy pressure is typically positive. On the other hand, for directional bonding with angular character, the Cauchy pressure is negative, with larger negative pressure representing a more directional character. These correlations have been verified for ductile materials such as Ni and Al that have typical metallic bonding, as well as for brittle semiconductors such as Si with directional bonding.⁴³ In the ionic compound KMgF_3 , the calculated Cauchy pressure is -10 GPa within LDA and -15 GPa within GGA, in good agreement with the nonmetallic characteristics of KMgF_3 .

Table III presents sound velocities as derived from the calculated elastic constants.²⁴ The calculated sound velocities agree quite well with the experiments, in particular, for the GGA values, which is a consequence of the somewhat fortuitous good agreement between the measured and GGA calculated elastic constants.

IV. ELECTRONIC STRUCTURE

The calculated electron band structure of KMgF_3 is shown in Fig. 3, with the ensuing density of states in Fig. 4. The valence bands consist of the Fp bands with a gap of 7.24 eV to the conduction band, which is dominated by K states. The LDA bands are almost identical, however, with a

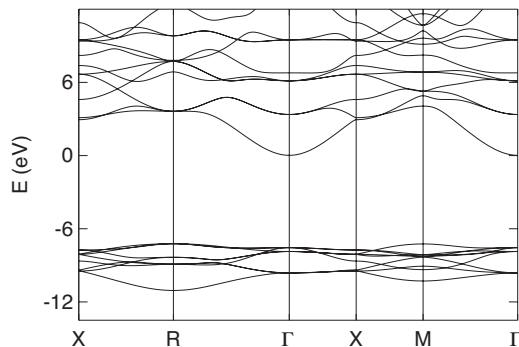


FIG. 3. Band structure of KMgF_3 (using GGA, at the experimental lattice constant). The zero of energy is set at the position of the conduction band minimum.

TABLE III. Calculated longitudinal, shear, and average wave velocities (v_l , v_s , and v_m , respectively) in m/s for KMgF_3 at the theoretical equilibrium volume.

		v_l	v_s	v_m
Present work	LDA	7402	4396	4870
	GGA	6706	4073	4507
Experiment		6470^a , 6540^b	3940^a , 3900^b	4290^c

^aWave vector along $\langle 100 \rangle$ direction (Ref. 12).

^bWave vector along $\langle 110 \rangle$ direction (Ref. 12).

^cReference 11.

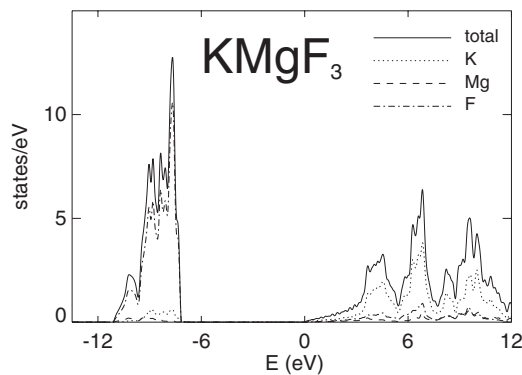


FIG. 4. Density of states of KMgF_3 (using GGA, at the experimental lattice constant). The zero of energy is set at the position of the conduction band minimum. The partial projections onto the spheres of K, Mg, and F are shown with dotted, dashed, and dash-dotted lines, respectively, while full line gives the total density of states. Units are electrons per eV and per f.u.

gap of only 6.95 eV. The gap increases almost linearly with compression, at the rate

$$V \frac{dE_g}{dV} = -7.1 \text{ eV}.$$

The conduction band minimum occurs at the Γ point, while the valence band maximum occurs at the R point $(1/2, 1/2, 1/2) \frac{2\pi}{a}$. The largest occupied energy level at the

M point $(1/2, 1/2, 0) \frac{2\pi}{a}$ is marginally lower (by ~ 0.02 eV) than the valence band maximum at R , and it remains lower throughout the pressure range studied here.

V. CONCLUSIONS

In conclusion, we find that pure cubic KMgF_3 is very stable under high compression. From our analysis, we also find that it is a brittle system and an indirect gap insulator whose gap increases with pressure.

ACKNOWLEDGMENTS

G.V., V.K., A.D., and B.J. acknowledge VR and SSF for financial support and SNIC for providing computer time. One of the authors (R.S.K.) is greatly indebted to his departed colleague Yongrong Shen for some help in collecting the data. The authors gratefully acknowledge the use of the HPCAT facility supported by DOE-BES, DOE-NNSA, NSF, and the W. M. Keck Foundation. HPCAT is a high-pressure collaborative access team among the Carnegie Institution, Lawrence Livermore National Laboratory, the University of Nevada Las Vegas, and the Carnegie/DOE Alliance Center. We thank Maddury Somarazulu and other HPCAT staff for technical assistance. This research was supported by the U.S. Department of Energy Cooperative Agreement No. DE-FC52-06NA26274 with the University of Nevada, Las Vegas.

*Corresponding author. vaithee@kth.se

- ¹T. Nishimatsu, N. Terakubo, H. Mizuseki, Y. Kawazoe, D. A. Pawlak, K. Shimamura, and T. Fukuda, *Jpn. J. Appl. Phys., Part 2* **41**, L365 (2002).
- ²G. H \ddot{u} rsch and H. J. Paus, *Opt. Commun.* **60**, 69 (1986).
- ³T. Fukuda, K. Shimamura, A. Yoshikawa, and E. G. Villora, *Opto-Electron. Rev.* **9**, 109 (2001).
- ⁴P. Dorenbos, *Phys. Rev. B* **62**, 15640 (2000).
- ⁵A. V. Gektin, I. M. Krasovitskaya, and N. V. Shiran, *Radiat. Meas.* **29**, 337 (1998).
- ⁶C. Furetta, F. Santopietro, C. Sanipoli, and G. Kitis, *Appl. Radiat. Isot.* **55**, 533 (2001).
- ⁷M. O'Keeffe and J.-O. Bovin, *Science* **206**, 599 (1979).
- ⁸J. N. Street, I. G. Wood, K. S. Knight, and G. D. Price, *J. Phys.: Condens. Matter* **9**, L647 (1997).
- ⁹A. E. van Arkel, *Physica (The Hague)* **5**, 166 (1925).
- ¹⁰H. Remy and F. Hansen, *Z. Anorg. Allg. Chem.* **283**, 277 (1956).
- ¹¹I. G. Wood, K. S. Knight, G. D. Price, and J. A. Stuart, *J. Appl. Crystallogr.* **35**, 291 (2002).
- ¹²H. M. Rosenberg and J. K. Wigmore, *Phys. Lett.* **24A**, 317 (1967).
- ¹³L. M. Reshchikova, *Sov. Phys. Solid State* **10**, 2019 (1969).
- ¹⁴L. E. A. Jones, *Phys. Chem. Miner.* **4**, 23 (1979).
- ¹⁵R. A. Heaton and C. C. Lin, *Phys. Rev. B* **25**, 3538 (1982).
- ¹⁶R. A. Heaton and C. C. Lin, *J. Phys. C* **18**, 3211 (1985).
- ¹⁷T. Nishimatsu, N. Terakubo, H. Mizuseki, Y. Kawazoe, D. A.

- Pawlak, K. Shimamura, N. Ichinose, and T. Fukuda, *Jpn. J. Appl. Phys., Part 1* **42**, 5082 (2003).
- ¹⁸G. Q. Huang, L. F. Chen, M. Liu, and D. Y. Xing, *J. Phys.: Condens. Matter* **15**, 4567 (2003).
- ¹⁹M. Sahnoun, M. Zbiri, C. Daul, R. Khenata, H. Baltache, and M. Driz, *Mater. Chem. Phys.* **91**, 185 (2005).
- ²⁰S. Y. Savrasov, *Phys. Rev. B* **54**, 16470 (1996).
- ²¹S. H. Vosko, L. Wilk, and M. Nusair, *Can. J. Phys.* **58**, 1200 (1980).
- ²²J. P. Perdew, K. Burke, and M. Ernzerhof, *Phys. Rev. Lett.* **77**, 3865 (1996).
- ²³F. Birch, *J. Appl. Phys.* **9**, 279 (1938).
- ²⁴V. Kanchana, G. Vaitheeswaran, A. Svane, and A. Delin, *J. Phys.: Condens. Matter* **18**, 9615 (2006).
- ²⁵V. Kanchana, G. Vaitheeswaran, and A. Svane, *J. Alloys Compd.* (to be published).
- ²⁶A. V. Chadwick, J. H. Strange, G. Ranieri, and M. Terenzi, *Solid State Ionics* **9-10**, 555 (1983).
- ²⁷Y. Zhao, *J. Solid State Chem.* **141**, 121 (1998).
- ²⁸R. W. Smith, W. N. Mei, J. W. Flocken, M. J. Dudik, and J. R. Hardy, *Mater. Res. Bull.* **35**, 341 (2000).
- ²⁹C. D. Martin, S. Chaudhuri, C. P. Grey, and J. B. Parise, *Am. Mineral.* **90**, 1522 (2005).
- ³⁰L. A. Muradyan, V. E. Zavodnik, I. P. Makarova, K. S. Aleksandrov, and V. I. Simonov, *Kristallografiya* **29**, 392 (1984).
- ³¹Y. R. Shen, R. S. Kumar, M. Pravica, and M. F. Nicol, *Rev. Sci.*

- Instrum. **75**, 4450 (2004).
- ³²A. P. Hammersley, S. O. Svensson, M. Hanfland, A. N. Fitch, and D. Häusermann, *High Press. Res.* **14**, 235 (1996).
- ³³W. B. Holzapfel, *J. Appl. Phys.* **93**, 1813 (2003).
- ³⁴A. Darabont, C. Neamtu, S. I. Fărcas, and G. Borodi, *J. Cryst. Growth* **169**, 89 (1996).
- ³⁵J. Lee, H. Shin, J. Lee, H. S. Chung, Q. W. Zhang, and F. Saito, *Mater. Trans.* **44**, 1457 (2003).
- ³⁶A. R. Chakhmouradian, K. Ross, R. H. Mitchell, and I. Swainson, *Phys. Chem. Miner.* **28**, 277 (2001).
- ³⁷H. Z. Liu, J. Chen, J. Hu, C. D. Martin, D. J. Weidner, D. Häusermann, and H. K. Mao, *Geophys. Res. Lett.* **32**, L04304 (2005).
- ³⁸A. Delin, L. Fast, B. Johansson, O. Eriksson, and J. M. Wills, *Phys. Rev. B* **58**, 4345 (1998).
- ³⁹Y. S. Zhao *et al.*, *Am. Mineral.* **79**, 615 (1994).
- ⁴⁰S. Asbrink, A. Waskowska, H. G. Krane, L. Gerward, and S. Olsen, *J. Appl. Crystallogr.* **32**, 174 (1999).
- ⁴¹S. F. Pugh, *Philos. Mag.* **45**, 823 (1954).
- ⁴²I. N. Frantsevich, F. F. Voronov, and S. A. Bokuta, *Elastic Constants and Elastic Moduli of Metals and Insulators Handbook*, edited by I. N. Frantsevich (Naukova Dumka, Kiev, 1983), pp. 60–180.
- ⁴³D. Pettifor, *Mater. Sci. Technol.* **8**, 345 (1992).